CHALMERS
UNIVERSITY OF TECHNOLOGY

Hydropower optimization with detailed reservoir representation

Novel approaches for accurate modeling of reservoir levels in hydropower river systems

Master's thesis in Engineering mathematics and computational science

Alfred Andersson
Holger Johansson

Department of Space, Earth and Environment
CHALMERS UNIVERSITY OF TECHNOLOGY
Gothenburg, Sweden 2025
www.chalmers.se

Master's thesis 2025

Hydropower optimization with detailed reservoir representation

Novel approaches for accurate modeling of reservoir levels in hydropower river systems

Alfred Andersson
Holger Johansson

CHALMERS
UNIVERSITY OF TECHNOLOGY

Department of Space, Earth and Environment
Division of Physical Reasearch Theory
Energy System Analysis
Chalmers University of Technology
Gothenburg, Sweden 2025

Hydropower optimization with detailed reservoir representation
Novel approaches for accurate modeling of reservoir levels in hydropower river systems
Alfred Andersson
Holger Johansson

Supervisor: Hanna Ek Fälth, Älvbyrån AB
Examiner: Fredrik Hedenus, Department of Space, Earth and Environment

Master's Thesis 2025
Department of Space, Earth and Environment
Division of Physical Research Theory
Energy System Analysis
Chalmers University of Technology
SE-412 96 Gothenburg
Telephone +46 31 772 1000

Cover: Akkats power plant, photo provided by Richard Sharff at Vattenfall AB.

Typeset in LaTeX
Printed by Chalmers Reproservice
Gothenburg, Sweden 2025

Hydropower optimization with detailed reservoir representation
Novel approaches for accurate modeling of reservoir levels in hydropower river systems

Alfred Andersson & Holger Johansson
Department of Space, Earth and Environment
Chalmers University of Technology

Abstract

Optimization models are commonly used to analyze long-term scenarios for hydropower production. These models rely on accurately representing how hydropower systems work to produce reliable results. However, reservoir water levels are often modeled in an overly simplified way, leading to unrealistic relationships between the stored water volume and the corresponding water level. This, in turn, can cause problems when incorporating environmental permits that depend on water levels. Therefore, this study focuses on improving the detail of water levels in both linear and nonlinear hydropower scenario analysis models. Specifically, by more realistic modeling of reservoir levels by incorporating nonlinear and linear approximations of reservoir level-volume data, referred to as reservoir curves.

Four enhanced models are proposed: two implement detailed reservoir curves directly via equality constraints in linear and nonlinear forms, while two use convex relaxations followed by post-optimization adjustments, also in both linear and nonlinear forms. The convex relaxation models, offering computational efficiency, are validated against the more exact equality constraint models. Validation results show that the relaxation-based models give solutions close to the stricter equality constrained models.

The proposed models with detailed water level modeling enable more scenarios using actual environmental permits than the models without. The resulting revenue and power production for full aggregated river systems do not show any notable difference between models that incorporate reservoir curves and models without them. However, the power production capacity of some individual power plants in river systems is affected by more detailed water level modeling.

Keywords: Hydropower, Modeling, Optimization, Head, Forebay levels, Reservoir curves, Environmental permits, Energy systems.

List of Acronyms

Below is the list of acronyms that have been used throughout this thesis listed in alphabetical order:

ILP	Integer Linear Program
INLP	Integer Nonlinear Program
IP	Integer Program
KKT	Karush-Kuhn-Tucker
LP	Linear Program
m.a.s.	Meters above sea level
MILP	Mixed Integer Linear Program
MINLP	Mixed Integer Nonlinear Program
MIP	Mixed Integer Program
Model A	Baseline nonlinear and nonconvex model
Model A:EQ	Nonlinear and nonconvex model with strictly enforced forebay levels (by equality constraints)
Model A:R	Nonlinear and nonconvex model with convex relaxation of forebay level constraints
Model B	Baseline linear and convex model
Model B:MILP	Mixed integer linear and nonconvex model with strictly enforced forebay levels (using binary variables)
Model B:R	Linear and convex model with convex relaxation of forebay level constraints
NLP	Nonlinear Program
ROG	Relative Optimality Gap
WFD	Water Framework Directive

Contents

List of Figures

List of Tables

1
Introduction

Reservoir hydropower is the single largest source of low-carbon energy worldwide [1]. In addition to delivering low-carbon energy, reservoirs allow for both short- and long-term energy storage capabilities. This allows energy to be dispatched on time scales ranging from seconds to seasons, giving flexibility to the overall energy system. This gives hydropower production a critical role in the transition to energy systems with a higher share of variable renewable energy (VRE) sources such as solar and wind [2][3]. To accurately assess the role of hydropower in the future, high-resolution hydropower optimization models with long time horizons and high technical detail are of great importance.

Although hydropower production is regarded as a benign energy technology as it emits virtually no CO_2 during operation, the impoundment of rivers significantly impacts ecosystems in and around the rivers and reservoirs. Natural water flow patterns are altered and connectivity is hindered, disrupting fish migration and sediment transport, which ultimately has cascading negative effects on biodiversity [4]. Consequently, members of the European Union must respect the Water Framework Directive (WFD) [5], which states that member states must have updated plans to ensure a good environmental status in water bodies. An example of the enforcement of the WFD was manifested in Sweden in 2024. The European Commission opened an infringement case against Sweden for insufficient progress in this regard [6], prompting revised environmental permits. To understand the impact on power production from revising permits, hydropower models that are capable of accurately representing water levels become crucial, since these permits constrain allowed flows and water levels in rivers.

Many hydropower optimization models simplify the non-linear link between reservoir water levels and reservoir content (water volume), a relationship that varies with each reservoir's geometry. Reservoirs are often assumed to have a simple rectangular block geometry, which makes water levels linearly depend on the volume [7][8][9]. When detailed level–volume representation is included, other dynamics are idealized, and authors rarely document either a detailed formulation or its practical effects, leaving an important research gap. Hjelmeland et. al. [10] briefly discuss the nonlinearity of the reservoir curves for Norwegian reservoirs but do not give an exhaustive formulation of how it is modeled. Barros et. al. [11] employ fourth degree polynomial functions to describe reservoir curves but do not provide a description of the shape of the functions or how they are constructed and use weekly time resolution. Yang et. al. [12] takes a data driven approach, fitting polynomials ranging from 8-14 degrees to reservoir curves but have simplified other aspects such as turbine efficiency, time horizon and resolution.

This thesis addresses long-term hydropower scenario analysis in river systems using deterministic optimization models. In particular, the study investigates how a more accurate representation of river reservoir water content and forebay level (surface level) relationship, called reservoir curves, can be incorporated into these models. Long-term in this context refers to a time horizon of months to years, and the model is deterministic in the sense that the model has perfect foresight in otherwise stochastic dynamics such as electricity prices and inflow. By integrating more accurate representations of reservoir curves, the resulting optimization models can better reflect the physical reality, which in turn enables meaningful modeling of environmental constraints.

1.1 Aim

To be able to model environmental permits, it is important that the water levels in reservoirs are correctly represented. The aim of this project is to investigate how detailed reservoir curve modeling affects the performance and outcomes of hydropower optimization. Hence, the specific aim of this project is to answer the following questions:

1. *How can reservoir curves, which represent the reservoir forebay level-reservoir content relationship, be mathematically represented?* The goal is to develop both linear and nonlinear expressions that accurately capture this dynamic.

2. *In what ways can reservoir curves be implemented in a hydropower optimization model?* Here, the purpose is to make the developed mathematical expressions work within the framework of a linear, convex, and a nonlinear, nonconvex optimization model.

3. *How does more detailed modeling of reservoir forebay levels affect the feasibility of modeling river hydropower environmental permits?* Current optimization models do not allow for feasible solutions while implementing some of today's real-world environmental permits. The goal is to model reservoir curves that enables this.

4. *How do more accurately modeled forebay levels affect modeled scenarios for large river networks?* Specifically, evaluation of the merits of the proposed implementation in terms of power and revenue in resulting solutions.

1.2 Case study: Five Swedish river systems

The new reservoir curve formulations were tested on five Swedish rivers: Ljungan, Luleälven, Umeälven, Dalälven, and Indalsälven, which span a wide range of installed capacity, network size, and reservoir topology. The choice of these rivers is motivated by three practical considerations:

1. **Data availability** - Vattenregleringsföretagen and Energiföretagen has kindly supplied reservoir curve measurements for these rivers, a prerequisite for accurate forebay level modeling.

2. **Regulatory relevance** - All of these rivers are subject to a revision of environmental permits in response to the infringement case, making them highly policy-relevant.

3. **Model continuity** - Two established hourly resolution hydropower optimization models (one convex, linear, one nonconvex, nonlinear) already cover these rivers. Implementing reservoir curves in these models allows for isolation of the effect of better forebay level representation without changing any other inputs. Furthermore, the established optimization models used as baseline are highly detailed, which allows for evaluation of how the implementation works for practical use in terms of computational complexity.

2
Background

To understand how to model reservoir hydropower, it is essential to understand the basic principles of the physics and types of constraints that apply. First, a simplified crash course on how electricity is produced in hydropower plants is given. This is followed by a brief overview of previous research and different types of optimization models.

2.1 Principles of hydropower

Hydropower plants convert potential energy of an elevated water mass into mechanical energy by rotating turbines which in turn produce electrical energy by a generator [13]. The potential energy is determined by the water column height called the head, which is the difference between the water level at the turbine inlet, called forebay level, and the water level at the turbine outlet, called tailrace level (see Figure 2.1). The head (H) along with the flow of water through the turbine, called the discharge (D), the turbine efficiency (η), gravitational constant (g), and water density (ρ) make up the power (P) produced by a turbine as:

$$P = D \cdot \eta \cdot H \cdot g \cdot \rho \qquad [W] \tag{2.1}$$

Reservoir hydropower plants can store and regulate the water flow by constructed dams. These plants are connected in a river network (see Figure 2.2) where production capacity depends on the operation of both upstream and downstream plants. Run-of-river stations can also exist in these networks with negligible storage and are effectively pass-through units. Pumped storage hydropower is another category of hydropower production but is outside the scope of this thesis.

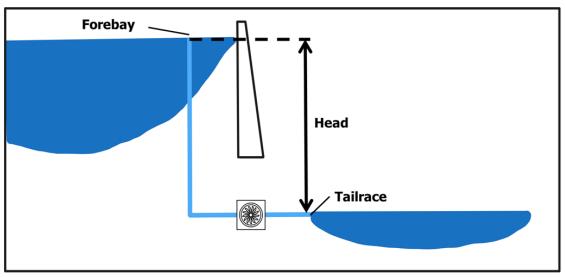

Figure 2.1: Simplified schematic of a hydropower plant, showcasing forebay level, tailrace level, and head.

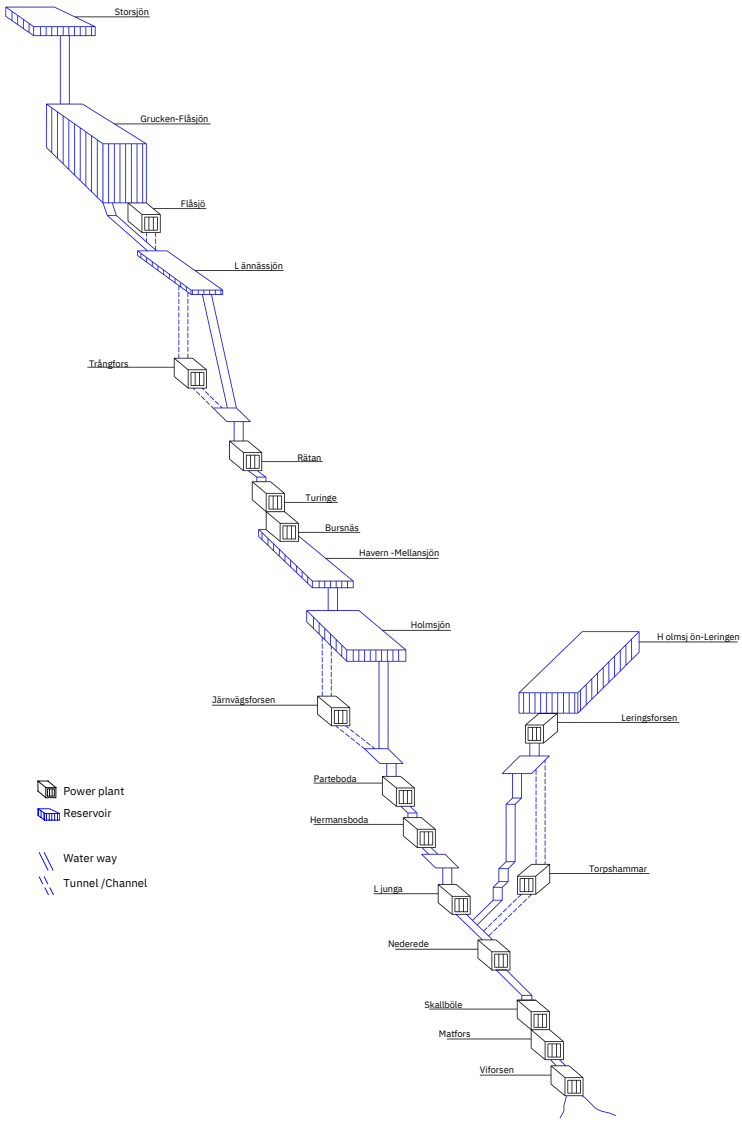

Figure 2.2: Network structure of the river Ljungan.

2.2 Different types of hydropower optimization models

Mathematical optimization modeling of hydropower is a tool that is generally used to evaluate real-world scenarios or to compute optimal production plans. An optimization model can be very different from another depending on its intended use. The level of detail incorporated is often dependent on the computational difficulty that inevitably comes with more detail. The main aspects affecting computational difficulty are time resolution and time horizon, deterministic or stochastic water inflow and price data, and the type of optimization problem (see Chapter 3). A brief and non-exhaustive literature review is presented in Table 2.1 to give an overview of different types of optimization models. The level of detail that the models investigated choose to include or not are in general:

- *Head dependency*, determines if the head of a turbine is variable with water surfaces. The way models calculate the forebay and tailrace levels vary between combinations of nonlinear, linear or constant functions.
- *Turbine efficiency*, the efficiency of a turbine can be assumed to be constant or dependent on water discharge.
- *River network*, models can evaluate one single reservoir with turbines or a network of reservoirs, dams, and power plants.

Table 2.1: A brief literature review of different optimization models for hydropower. Linear head refers to the forebay and tailrace levels being modeled with linear functions while nonlinear refers to one or both of these having a nonlinear function.

Model	Type	Time	Head	Turbine eff.	Network
Barros et. al.[11]	Deterministic, Long-term scheduling	Monthly resolution, year	Variable (nonlinear)	Constant	Large, 39 reservoirs
Catalão et. al.[7]	Deterministic, Short-term scheduling	Hourly resolution, 1 week	Variable (linear)	Variable (linear)	Medium, 7 reservoirs
Ek Fälth et. al.[8]	Deterministic, Scenario analysis	Hourly resolution, 1 year	Variable (linear)	Variable (nonlinear)	Large, 17 reservoirs
Goor et. al.[14]	Stochastic, Long-term scheduling	Monthly resolution, 5 years	Variable (piecewise linear)	Variable (linear)	Medium, 14 reservoirs
Guisández et. al.[15]	Deterministic, Scenario analysis	Weekly resolution, 1 year	Variable (linear)	Variable (piecewise linear)	Small, 1 reservoir
Hjelmeland et. al.[10]	Stochastic, Long-term scheduling	Weekly resolution, 2 years	Variable (imprecise description)	Variable (piecewise bi-linear)	Small, 3 reservoirs
Yang et. al.[12]	Deterministic, Mid-term scheduling	Daily resolution, 1 month	Variable (nonlinear)	Constant	Small, 3 reservoirs
Zhou et. al.[9]	Deterministic, Long-term scheduling	Monthly resolution, year	Variable (piecewise linear)	Constant	Small, 4 reservoirs

In the paper *Trade-offs between aggregated and turbine-level representations of hydropower in optimization models* by Ek Fälth et. al. [8] a novel type of hydropower optimization model is presented. The nonlinear (Section 3.4) and non-convex (Definition 3.6) optimization model Model A includes river network effects, turbine efficiency curves, and head dependency while allowing for mid- to long-term time horizons with hourly resolution. A linear (Section 3.3) and convex (Definition 3.6) model including a similar level of detail is given in Model B:L as described in [8], simply referred to as Model B hereinafter. Because of the level of overall detail in Model A and Model B, long-term time horizon, and high resolution, these models are used as the basis when analyzing how more detailed reservoir curve modeling affects hydropower optimization models. Currently, Model A and Model B model the reservoir curves linearly, which essentially means that the reservoir geometry is assumed rectangular. Figure 2.3 illustrates how the geometry of idealized reservoirs can be represented by reservoir curves.

Using models Model A and Model B it is not possible to model all real world environmental constraints due to idealized reservoir curve modeling. Enabling true modeling of environmental permits is essential for the models' practical use, and

hence it is a crucial part of this project's aim to develop the models to include realistic reservoir curves.

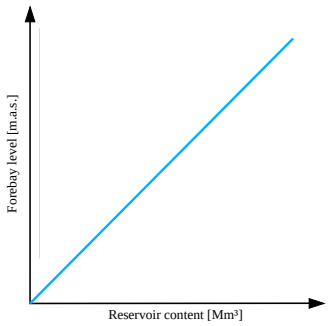

(a) Linear assumption of reservoir curve for the operating range.

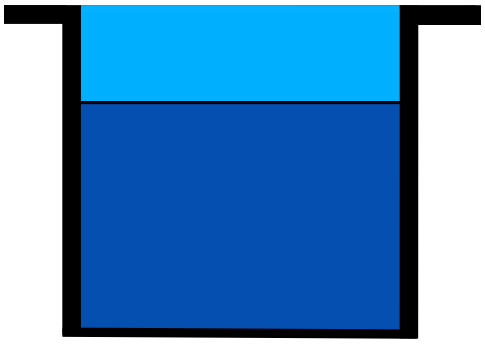

(b) A schematic representation of the cross section of a linear reservoir, the operating range is highlighted by the light blue region.

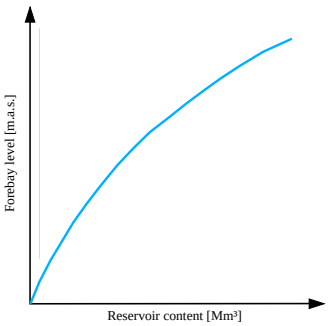

(c) A concave and nonlinear reservoir curve for the operating range. This is how most reservoirs appear to be in reality.

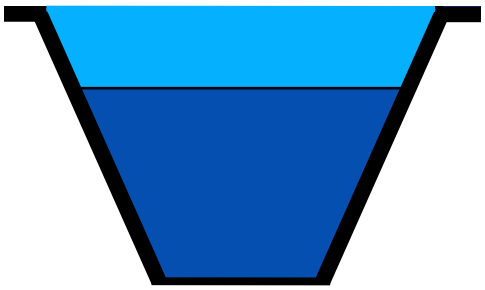

(d) A schematic representation of the cross section of nonlinear, concave reservoir, the operating range is highlighted by the light blue region.

Figure 2.3: Schematic representations of different reservoir curves and possible cross sections. This is highly idealized since reservoirs are three dimensional. The figure is intended to give an intuition for different reservoir curve shapes.

The majority of environmental permits connected to water levels regulate the lower bound of the allowed operating region for reservoirs. Enforcing these permits in a model using a linearized reservoir curve assumption results in overly strict constraints of the operating range (see Figure 2.4). This is problematic for two reasons: The effects of environmental permits could be exaggerated, and the overall feasibility of the problem could be compromised if other environmental flow permits and local inflow data do not support this tighter range of reservoir content operating range.

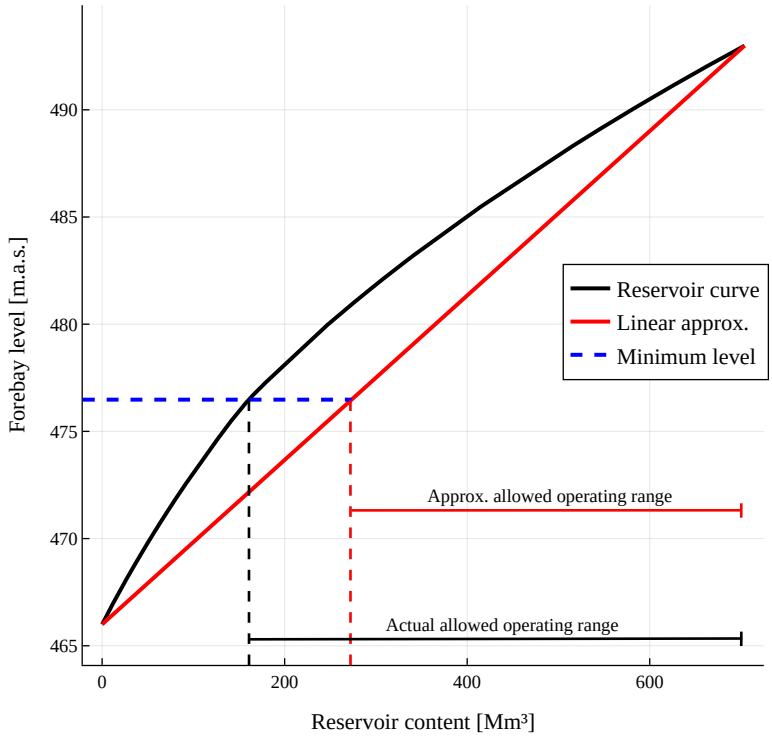

Figure 2.4: Actual reservoir curve data and linear assumption of reservoir curve. An example minimum forebay level environmental permit is displayed with the resulting allowed operating regions in terms of reservoir content.

3

Optimization theory

This chapter briefly introduces the field of mathematical optimization theory in general, including some key concepts such as convexity, types of optimal solutions, and different classes of optimization problems.

3.1 Basic terminology

Let the notation

$$\begin{array}{lll} \text{minimize} & f(x) & \\ \text{subject to} & g_i(x) \leq 0, & i = 1, \ldots, m \\ & h_j(x) = 0, & j = 1, \ldots, n \\ & x \in S & \end{array} \tag{3.1}$$

describe the optimization problem of finding an x from the set $S \subseteq \mathbb{R}^d$ that minimizes the objective function $f(x)$ while satisfying the inequality constraints $g_i(x)$ and equality constraints $h_j(x)$. This notation is used as a reference problem for following theory, the minimization problem type is used due to most optimization theory being defined from this notation. Any maximization problem can be written as a minimization problem as maximizing $-f(x)$ is equal to minimizing $f(x)$.

Definition 3.1 (Global optimum [16]) *Consider the problem* (3.1) *and let* $x^* \in S$*. We say that* x^* *is a global optimum (minimum) of* f *if*

$$f(x^*) \leq f(x), \quad \forall\ x \in S \tag{3.2}$$

holds.

Intuitively, a global optimum is the best point out of all the feasible points in a set.

Definition 3.2 (Local optimum [16]) *Consider the problem* (3.1) *and let* $x^* \in S$*. Let* $B_\varepsilon(x^*) := \{y \in \mathbb{R}^d \mid ||y - x^*|| < \varepsilon\}$ *be the open Euclidean ball with radius* ε *centered at* x^**. We say that* x^* *is a local optimum (minimum) of* f *on the set* S *if*

$$\exists\ \varepsilon > 0 \text{ such that } f(x^*) \leq f(x), \quad \forall\ x \in S \cap B_\varepsilon(x^*) \tag{3.3}$$

This is a technical way of saying that if for a small vicinity around x^* there is no $x \in S$ that has an objective function value better than x^*, then x^* is a local optimum.

3.2 Convexity

Definition 3.3 (Convex set [16]) *Let $S \subseteq \mathbb{R}^d$. The set S is convex if*

$$\lambda x_1 + (1 - \lambda)x_2 \in S \tag{3.4}$$

is true for all $x_1, x_2 \in S$ and all $\lambda \in (0, 1)$.

This means that when picking any two points from a convex set S, every point on the line segment between them also lies within S.

Definition 3.4 (Convex function [17]) *Let $S \subseteq \mathbb{R}^d$ be a convex set. A function $f : \mathbb{R}^d \to \mathbb{R}$ is said to be a convex function on S if*

$$f(\lambda x_1 + (1 - \lambda)x_2) \leq \lambda f(x_1) + (1 - \lambda)f(x_2) \tag{3.5}$$

In other words, a convex function is always below or equal to (in terms of function value) the linear interpolation.

Definition 3.5 (Concave function [16]) *A function $f : \mathbb{R}^d \to \mathbb{R}$ is said to be concave on a convex set S if $-f$ is convex.*

A concave function is always above or equal to the linear interpolation. Note that linear functions are both convex and concave.

Definition 3.6 (Convex optimization problem [17]) *A convex optimization problem is one of the form (3.1) where the objective function is convex and all the constraints construct a convex feasible region. This is achieved for a minimization (maximization) problem when*

1. *The objective function is convex (concave).*
2. *Inequality constraint functions are convex (concave).*
3. *Equality constraint functions are affine.*

Definition 3.7 (Fundamental theorem of global optimality [16]) *Consider the problem (3.1), where $f(x)$ is convex, $g_i(x)$ $i = 1, \ldots, m$ are convex, and $h_j(x)$ $j = 1, \ldots, n$ are affine, making it a convex optimization problem. Then, every local optimum of f is also a global optimum.*

This is a very powerful theorem, since it ensures that the solution found is guaranteed to be the best possible solution to the formulated problem. In nonconvex problems, a large difficulty is deciding when to settle for a "good enough" solution (local optimum). In convex problems, we do not have this problem. It should be noted that, for many applications of optimization problems, hunting for a global optimum that is a marginal improvement from another local one has little effect on the usefulness of the solution, since the model itself often contains idealizations and approximations.

3.3 Linear programming

Linear programming (LP) is an important class of optimization problems. In linear programs, the objective function and all constraints are linear, constructing polyhedral feasible regions which are always convex (Definition 3.3). The main appeal to LP models is that they can be solved to global optimum (Definition 3.1 and 3.7) and there exist efficient algorithms for solving them. The most used being simplex [18], and barrier methods [19], also known as interior point methods.

3.4 Nonlinear programming

Nonlinear programming (NLP) is the class of optimization problems where the objective function or constraint functions are nonlinear. Solving nonlinear programs are typically much more challenging compared to LP problems. Methods for local optimization require differentiability of objective and constraint functions, and typically rely on the Karush-Kuhn-Tucker (KKT) conditions [20] to prove local optimality (Definition 3.2). Global optimality can rarely be proven unless the problem is convex (Definition 3.6).

Nonlinear solution algorithms for local optimization typically require an initial guess for the optimization variables. The choice of this guess is critical as the algorithm can get stuck at quite poor local optima, conversely, a good initial guess can guide the algorithm to finding a good local optimum. A common practice is to solve a convexified and sometimes linearized version of the problem first and use this as the initial guess. This is referred to as a warm start. For example, one reason to create Model B was to use it as warm start for Model A. Hence, it is important to continue the develop these models in parallel for this project as well.

3.5 Mixed integer programming

Mixed integer programming (MIP) refers to a class of optimization problems that contain both continuous and integer variables. There are also pure integer programs (IP), integer linear programs (ILP), mixed integer linear programs (MILP), integer nonlinear programs (INLP), and mixed integer nonlinear programs (MINLP). Integer variables can be useful in model formulations where the real-world problem that is modeled contain features that does not make sense to take decimal values, e.g. when optimizing how many turbines to install in a hydropower plant, an answer of 4.6 turbines is not very useful. Binary integer variables (variables of the set $\mathbb{B} := \{0, 1\}$) are also useful in modeling as they can be used as on/off gates to represent a selection and only apply specific constraints depending on this selection.

There are many solution methods for MIP, most algorithms in some stage rely on the Branch and Bound algorithm [21]. This algorithm can in theory always solve to global optimality (if the continuous relaxation is convex) by enumerating all possible integer feasible solutions. This is however rarely a realistic approach. Suppose there are n binary variables, to evaluate all the integer feasible solutions uses n computer operations. Since there are 2 choices for each variable, this results

in 2^n operations. With 100 binary variables, this amounts to over 10^{30} operations. For reference, the state of the art super computer El Capitan [22] can perform 10^{18} operations per second, meaning it would take roughly 31,000 years to compute. MIP solvers instead settle for a tolerable solution, usually determined by how close the best integer feasible objective is to the continuous relaxation objective.

4
Method

First, this chapter presents an overview of the nonlinear and nonconvex Model A and linear and convex Model B proposed by Ek Fälth et. al. [8], in which the reservoir level representation is improved in this study. Next, the mathematical formulations developed to capture the forebay levels with higher physical realism, answering research question number one, are presented. Following this, four new model implementations are presented based on these forebay level formulations, answering research question number two. Finally, a description of the modeled scenarios used for model validation and comparison is given.

4.1 Overview of Model A and Model B

This section describes Model A and Model B which are used as building blocks for all models presented in the following section. The only difference between these models and the new models proposed later is how the forebay level constraint (4.10) is handled. The notation for the model formulations is summarized in the model nomenclature below, variables are denoted by uppercase letters, and parameters in lowercase.

Model nomenclature

Indices

h	Hour
n	Power plant
j	Turbine
un	Upstream plant
dn	Downstream plant
F	Forebay
T	Tailrace

Variables

R	Revenue from selling electricity
P	Power production
V	Reservoir content
D	Discharge
S	Spilled water
H	Head
W^F	Forebay water level
W^T	Tailrace water level
Z	Binary decision variable
Y	Reservoir content auxiliary variable

Parameters

p_i	Electricity price
ρ	Water density
g	Gravitational constant
$\bar{h}$	Mean head
$\bar{e}$	Mean effective discharge
i	Inflow
δ	Flow delay time
v^{max}	Maximum reservoir content
v^{start}	Start reservoir content
v^{end}	End reservoir content
β	Regression coefficient
s^{min}	Minimum allowed spilled flow
d^{min}	Minimum allowed total flow
w^{min}	Minimum allowed forebay level
w^{max}	Maximum allowed forebay level
w^F	Forebay level data
v	Reservoir content data
a	Linear segment intercept
b	Linear segment slope

Functions

f^P	Power production function
f^E	Effective discharge function
f^{Fj}	Nonlinear forebay level fits
f^{F*}	Best Nonlinear forebay level fit
f^{FL}	Piecewise linear approximation of f^{F*}

4.1.1 Objective function

Maximizing the total revenue (R) across all hours (h), plants (n) and turbines (j) is set as the objective function for all models, computed as a product of hourly, plant- and turbine-wise power production (P) and the historical hourly market electricity

price (p_h) summed for all plants, turbines and hours.

$$R^* = \max \sum_{h,n,j} P_{h,n,j} \cdot p_h \tag{4.1}$$

4.1.2 Constraints

Constraints described below are generalized and apply to all hours, plants, and turbines. Note that not all plants have turbines, some are just reservoirs with dams to regulate the water flow.

(1) Power production
The power production is proportional to the water density (ρ), gravitational constant (g), head (H), discharge (D) and turbine efficiency ($\eta(D)$). The turbine efficiency and discharge is combined into the effective discharge variable (E). The power production function is defined as:

$$P_{h,n,j} \leq f^P_{h,n,j}(E_{h,n,j}, H_{h,n}) \cdot \rho \cdot g \tag{4.2}$$

In Model A, $f^P_{h,n,j}$ is a bilinear function defined as:

$$f^P_{h,n,j}(E_{h,n,j}, H_{h,n}) = E_{h,n,j} \cdot H_{h,n,j} \tag{4.3}$$

while in Model B, it is linearized as:

$$f^P_{h,n,j}(E_{h,n,j}, H_{h,n}) = \left(E_{h,n,j} \cdot \bar{h}_n + \bar{e}_{n,j} \cdot H_{h,n} - \bar{e}_{n,j} \cdot \bar{h}_n\right) \tag{4.4}$$

where $\bar{h}$ and $\bar{e}$ are historical mean values for the head and effective discharge respectively.

(2) Effective discharge
For exact details on the effective discharge functions f^E see [8]. In Model A a quadratic fit is employed to $\eta(D) \cdot D$ from historical turbine operation data. In Model B, this is instead approximated by several linear segments. The general constraint is formulated as:

$$E_{h,n,j} \leq f^E_{h,n,j}(D_{h,n}) \tag{4.5}$$

Note that both (4.2) and (4.5) are defined as inequality constraints to facilitate the robustness of the optimization solver but are fulfilled with equality in the solution since both variables are included in the objective function, pushing them to be as large as possible.

(3) Water balance
The reservoir content (V) is modeled as the reservoir content the previous hour, added with the inflow (i), upstream plant discharge (D) and spilled water (S), and subtracted by the plant discharge and spilled water. The upstream flows are delayed

by a time δ which is based on historical data on the time it takes for water to run from an upstream plant un to plant n rounded to the nearest integer.

$$V_{h,n} = V_{h-1,n} + 1 \left(i_{h,n} - \sum_j D_{h,n,j} - S_{h,n} + \sum_j D_{h-\delta_n,un,j} + S_{h-\delta_n,un} \right) \tag{4.6}$$

The multiplication of 1 represents one hour to ensure correct units. Reservoir content is defined from 0 at the reservoirs minimum operating range to the maximum possible content (v^{max}).

$$0 \leq V_{h,n} \leq v_n^{max} \tag{4.7}$$

Reservoir content has boundary conditions for the first and last timestep, setting the reservoir content of all reservoirs to match historical data. The historical data are specific forebay levels at historical dates, this is converted to reservoir content values v^{start} and v^{end} by taking the inverse of (4.10).

$$V_{1,n} = v_n^{start} \tag{4.8}$$

$$V_{end,n} = v_n^{end} \tag{4.9}$$

(4) Water level constraints
The forebay level (W^F) is assumed to be linearly dependent on the reservoir content with coefficients β^F. The tailrace level (W^T) depends on the plant design, discharge, and downstream forebay level. The coefficients β^T are the result of linear regression from historical data.

$$W_{h,n}^F = \beta_0^F + \beta_1^F \cdot V_{h,n} \tag{4.10}$$

$$W_{h,n}^T = \beta_0^T + \beta_1^T \cdot \sum_j D_{h,n,j} + \beta_2^T \cdot W_{h,dn}^T \tag{4.11}$$

The head (H) is the difference between forebay and tailrace levels.

$$H_{h,n} = W_{h,n}^F - W_{h,n}^T \tag{4.12}$$

(5) Environmental constraints
Environmental permits can be modeled by setting time-specific constraints on spilled flow (s_{min}), total flow (d_{min}), maximum and minimum forebay levels (w^{max}, w^{min}).

$$s_{h,n}^{min} \leq S_{h,n} \tag{4.13}$$

$$d_{h,n}^{min} \leq \sum_j D_{h,n,j} + S_{h,n} \tag{4.14}$$

$$w_{h,n}^{min} \leq W_{h,n}^F \leq w_{h,n}^{max} \tag{4.15}$$

4.2 Forebay levels

This section addresses the first research question: *How can reservoir curves, which represent the reservoir forebay level-reservoir content relationship, be mathematically represented?* Here, methods to model forebay levels more accurately are presented,

while the resulting improvements are presented in Section 5.1. These different methods will later be incorporated into new versions of the hydropower optimization models Model A and Model B. Using data consisting of measurements $i = 1, \ldots, m$ of forebay levels $w^F_{i,n}$ coupled with reservoir content values $v_{i,n}$ for reservoir n, a fit was made to create functions for forebay levels depending on reservoir content, let this function be f^{F*}_n. To construct f^{F*}_n, multiple different fits were constructed for each reservoir:

$$f^{F1}_n(\boldsymbol{v}_n) = \beta^F_{0,n} + \beta^F_{1,n} \cdot \boldsymbol{v}_n \tag{4.16}$$
$$f^{F2}_n(\boldsymbol{v}_n) = \beta^F_{0,n} + \beta^F_{1,n} \cdot \boldsymbol{v}_n + \beta^F_{2,n} \cdot \boldsymbol{v}^2_n \tag{4.17}$$
$$f^{F3}_n(\boldsymbol{v}_n) = \beta^F_{0,n} + \beta^F_{1,n} \cdot \boldsymbol{v}_n + \beta^F_{2,n} \cdot \boldsymbol{v}^2_n + \beta^F_{3,n} \cdot \boldsymbol{v}^3_n \tag{4.18}$$
$$f^{F4}_n(\boldsymbol{v}_n) = \beta^F_{0,n} + \beta^F_{1,n} \cdot \boldsymbol{v}_n + \beta^F_{4,n} \cdot \sqrt{\boldsymbol{v}_n} \tag{4.19}$$
$$f^{F5}_n(\boldsymbol{v}_n) = \beta^F_{0,n} + \beta^F_{1,n} \cdot \boldsymbol{v}_n + \beta^F_{2,n} \cdot \boldsymbol{v}^2_n + \beta^F_{4,n} \cdot \sqrt{\boldsymbol{v}_n} \tag{4.20}$$

Each fit $f^{Fj}_n,\ j = 1, 2, 3, 4, 5$ was computed by solving the constrained least squares problem:

$$\begin{aligned} \min \quad & \sum_i \left(w^F_{i,n} - f^{Fj}_n(v_{i,n}) \right)^2 \\ \text{s.t.} \quad & f^{Fj}_n(v_{1,n}) = w^F_{1,n} \\ & f^{Fj}_n(v_{m,n}) = w^F_{m,n} \end{aligned} \tag{4.21}$$

where min and max forebay levels are strictly enforced. This is to ensure the end ranges of the operational range are accurately captured in the fits. Note that f^{F1}_n is exactly the same function as (4.10). Some examples of fits produced for a reservoir are presented in Figure 4.1.

Of the fits f^{Fj}_n, those that were strictly increasing and concave were kept. Then the one with the lowest sum of squared errors was selected as f^{F*}_n. The fit had to be strictly increasing to avoid that two different values of reservoir content could correspond to the same forebay level. This is a problem when computing start and end reservoir volumes. The choice of only using concave (Definition 3.5) fits is to allow for the implementation of a convex feasible region (Definition 3.3).

A linearization of f^{F*}_n was made by using piecewise linear segments $l = 1, \ldots, m$ between breakpoints $\hat{v}_{l,n}$ and $\hat{v}_{l+1,n}$, this gives a piecewise linear function f^{FL}_n (see Figure 4.2) for the forebay levels:

$$f^{FL}_n(V_{h,n}) = \begin{cases} a_{1,n} + b_{1,n} \cdot V_{h,n}, & \text{for } \hat{v}_{1,n} \leq V_{h,n} \leq \hat{v}_{2,n} \\ a_{2,n} + b_{2,n} \cdot V_{h,n}, & \text{for } \hat{v}_{2,n} \leq V_{h,n} \leq \hat{v}_{3,n} \\ \ldots & \\ a_{m,n} + b_{m,n} \cdot V_{h,n}, & \text{for } \hat{v}_{m,n} \leq V_{h,n} \leq \hat{v}_{m+1,n} \end{cases} \tag{4.22}$$

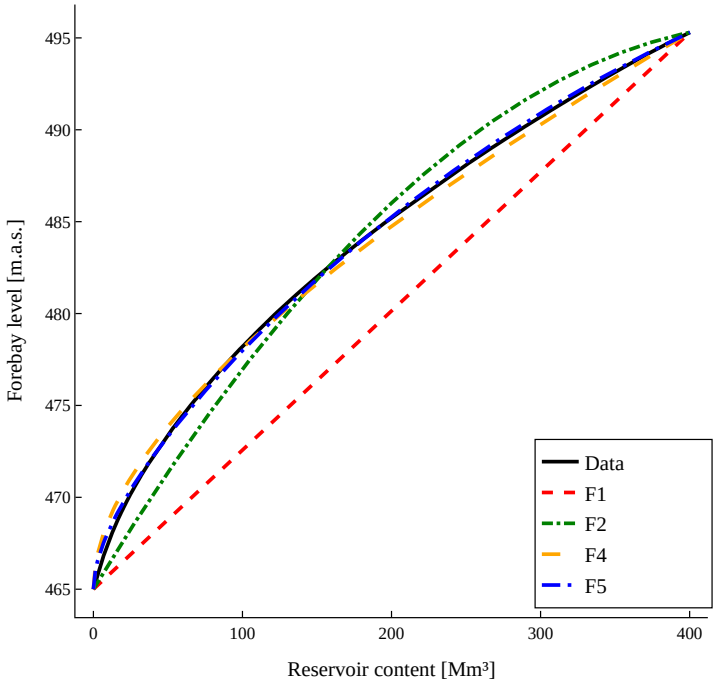

Figure 4.1: Example nonlinear fit of the forebay-volume data. Here the quadratic fit with a square root term f_n^{F5} would be selected as f_n^{F*}

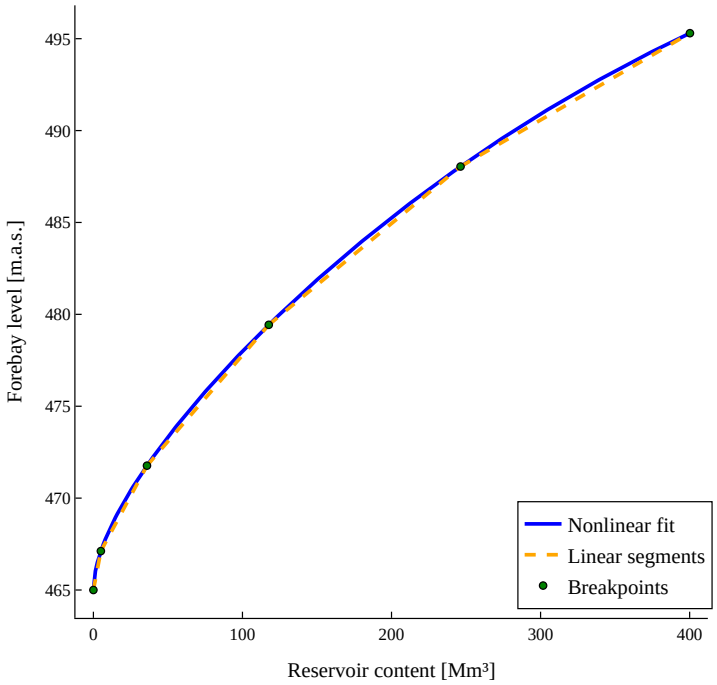

Figure 4.2: Example linearization $f_n^{FL}$of the forebay-volume fit.

4.3 Hydropower optimization models with improved reservoir level representation

In this section, four new model versions based on Model A and Model B are presented. The new proposed models seek to answer research question number two: *In what ways can reservoir curves be implemented in a hydropower optimization model?* The versions based on Model A are called Model A:R and Model A:EQ, and the versions based on Model B are called Model B:R and Model B:MILP. All model versions discussed in the thesis are summarized in Table 4.1 and presented in detail in Sections 4.3.1-4.3.4. The reason for presenting four new model versions, two nonlinear and two linear, is that the most obvious model versions turn out to be too computationally expensive. The new model versions Model A:EQ and Model B:MILP cannot be solved in reasonable time for one-year periods on a laptop (for reference, in some problems, no solutions were found after running the solver for five days on a computer with 64 GB memory and a Intel Core I9 3.5 GHz processor). To be able to conduct full scenario analysis for full river networks, it is crucial to analyze long time periods to capture all seasons and long-term effects, which Model A:EQ and Model B:MILP are incapable of.

Table 4.1: A summary of the models used in this study.

Model	Type	Convex	Purpose
Model A	NLP	no	Baseline NLP model.
Model B	LP	yes	Baseline LP model.
Model A:R	NLP	no	Improved NLP model.
Model B:R	LP	yes	Improved LP model.
Model A:EQ	NLP	no	Validate Model A:R.
Model B:MILP	MILP	no	Validate Model B:R.

Therefore, we developed two relaxed models Model A:R and Model B:R that are more computationally efficient. The two model versions Model A:EQ and Model B:MILP are used to verify that the models Model A:R and Model B:R give sufficiently similar solutions. The reason they might not is because these models recalculate the solution post-optimization, which means that the solution strays from an optimal one. The resulting water balance and flows may be different in the solutions produced by Model A:R and Model B:R compared to Model A:EQ and Model B:MILP where the forebay levels are set as equality constraints. Thus, the robustness of the models Model A:R and Model B:R will be validated against their corresponding equality model in Section 5.2 to fully answer the research question posed.

As presented in Section 3.4, a technique to remedy some of the computational difficulty of complex models is to use the solution of a simpler model as a warm start. This project follows this pattern and utilizes the simplicity of LP by setting the solution of Model B:R as a warm start for the models Model A:EQ, Model A:R, and Model B:MILP.

4.3.1 Model A:EQ

The first new model proposed is Model A:EQ. This model formulation explicitly enforces the forebay level functions by equality constraints:

$$W_{h,n}^{F} = f_{n}^{F*}(V_{h,n}) \tag{4.23}$$

This is a nonconvex constraint (except for linear f_n^{F*}). The nonconvex constraints add more complexity for the solver by introducing more local optima (Definition 3.2), making the problem more difficult to solve. In all other aspects, it is equal to Model A.

4.3.2 Model A:R

This model introduces a convex relaxation of (4.23), constructing a convex feasible region for the forebay levels. This is done by changing (4.23) to an upper bound, then utilizing the linear f_n^{F1} as a lower bound. The region between these functions is a convex region (see Figure 4.3):

$$\beta_0^F + \beta_1^F \cdot V_{h,n} \leq W_{h,n}^F \leq f_n^{F*}(V_{h,n}) \tag{4.24}$$

Post-optimization, W^F are projected onto f^{F*}, adjusting head H, tailrace level W^T, power production P, and revenue R accordingly while remaining feasible to the original problem. Ensuring convexity in the forebay constraints significantly improves the solver performance. In summary, Model A:R is equal to Model A in all aspects except the forebay level modeling and the post-optimization recalculation of variables.

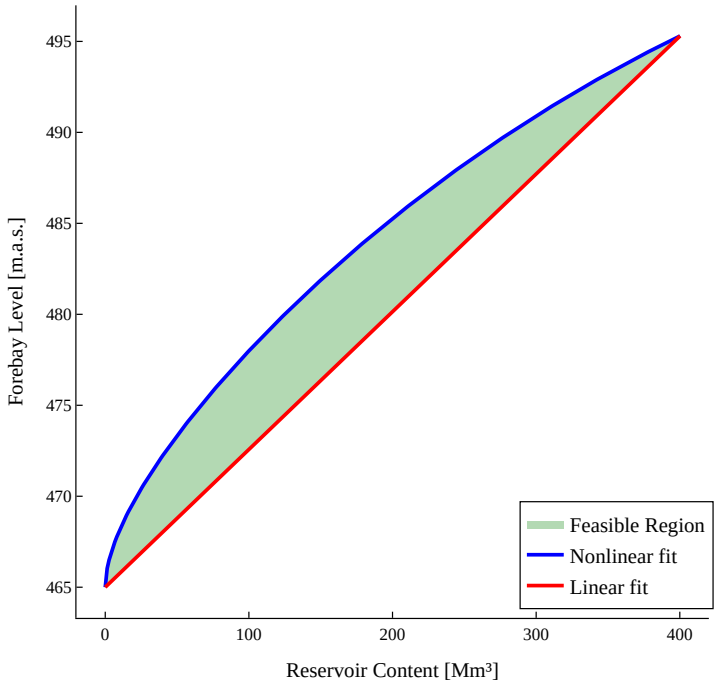

Figure 4.3: Visualization of the feasible region for forebay levels in Model A:R.

4.3.3 Model B:MILP

The first linear model presented is Model B:MILP. This model is equal to Model B except the formulation of forebay levels which makes this model a MILP. A MILP formulation explicitly sets forebay levels to specific linear segments from f_n^{FL} using binary selection variables $Z_{h,n,l}$ and auxiliary continuous variables $Y_{h,n,l}$. Whenever $Z_{h,n,l} = 1$, segment l is enforced. Similar to Model A:EQ, this ensures correct forebay levels but at the cost of greater computational demand. The formulation is as follows:

$$W_{h,n}^F = a_l \cdot \sum_l Z_{h,n,l} + b_l \cdot Y_{h,n,l} \tag{4.25}$$

$$Z_{h,n,l} \cdot v_l \leq Y_{h,n,l} \leq Z_{h,n,l} \cdot v_{l+1}, \qquad l = 1, \ldots, m \tag{4.26}$$

$$\sum_l Y_{h,n,l} = V_{h,n} \tag{4.27}$$

$$\sum_l Z_{h,n,l} = 1 \tag{4.28}$$

4.3.4 Model B:R

Instead of the MILP formulation of the forebay levels, this model use a larger feasible region. The same convex relaxation strategy as in Model A:R is applied but now using piecewise linear segments f_n^{FL} as an upper bound and a the same linear lower bound f_n^{F1} (see Figure 4.4). The forebay level constraints are formulated as:

$$\beta_0^F + \beta_1^F \cdot V_{h,n} \leq W_{h,n}^F \leq a_l + b_l \cdot V_{h,n}, \quad l = 1, \ldots, m \tag{4.29}$$

Post-optimization, projection of W^F onto f^{FL} is done similarly as Model A:R. The other variables head H, tailrace level W^T, power production P, and revenue R are recalculated accordingly using the definitions of Model B to ensure a feasible final solution.

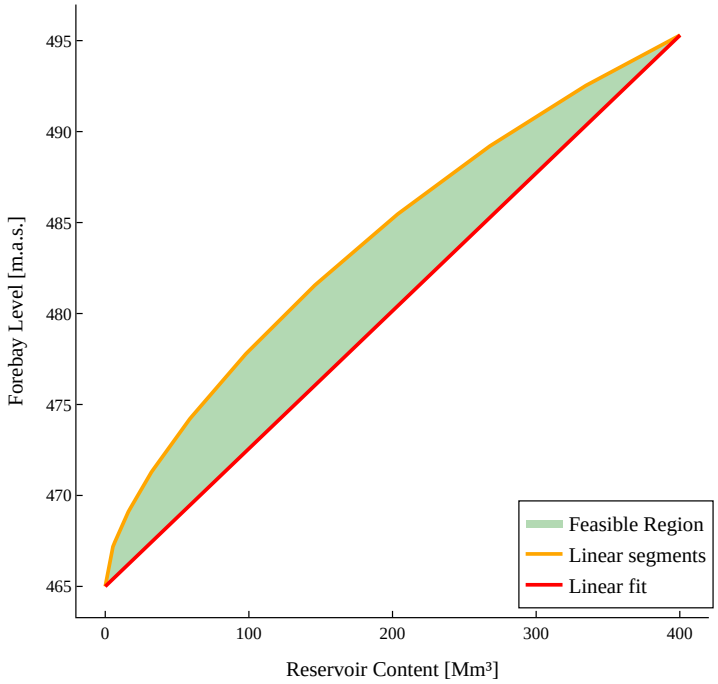

Figure 4.4: Visualization of the feasible region for forebay levels in Model B:R.

4.4 Modeled scenarios

The study uses data from five large rivers in Sweden: Ljungan, Umeälven, Luleälven, Dalälven, and Indalsälven (Table 4.2). Together, they contain 133 reservoirs, where some lack reservoir curve data and many have too small operating range to store water, making them effectively act as pass-through units. Because a detailed forebay function would add no practical value for such cases, a detailed reservoir curve is incorporated only for 33 reservoirs, while the remainder are represented by the linear approximation. Hourly historical inflows and spot prices (retrieved from NordPool) were taken for the two years 2016 and 2020 which were dry and wet years respectively.

Table 4.2: Rivers, number of reservoirs with nonlinear reservoir curve data, number of reservoirs and installed capacity included in the testing data set.

River	NL. reservoir curves	Reservoirs	Installed capacity (MW)
Ljungan	6	17	606
Umeälven	5	19	1758
Luleälven	5	18	4229
Dalälven	11	40	1136
Indalsälven	6	39	2154
Total	33	133	9883

The models Model A:R and Model B:R are validated against their more exact,

equality constrained, counterparts Model A:EQ and Model B:MILP. Because the more exact models are hard to solve for long time horizons, this test is limited to March in both years studied. March is chosen because reservoir levels are low and this is generally the region where the difference between the reservoir curves and the previous linear forebay level approximation is the largest. Each March is evaluated twice: Once with historical spot prices and once with an extreme price profile. The extreme price profile is synthetically constructed, where the variation in prices in 2016 and 2020 is amplified to represent hypothetical scenarios with extreme prices. The reason for including this additional price series is to get more robust results.

After the validation step, Model A:R and Model B:R are compared with the baseline models Model A and Model B for the entire years 2016 and 2020, using only historical prices.

5
Results and discussion

The results are divided into four sections, each in corresponding order to the research questions posed. The first two research questions are partially answered in the methods presented in Sections 4.2 and 4.3, respectively. The data and scenarios used are presented in detail in Section 4.4.

5.1 Forebay level functions

To fully answer the first research question: *How can reservoir curves, which represent the reservoir forebay level-reservoir content relationship, be mathematically represented?* This section provides results on how good the functions presented in Section 4.2 are in terms of fit to the data and compared with the linear fits used in the previous model versions Model A and Model B.

To measure how well the selected nonlinear fits explain the reservoir curve data, the R^2 is calculated. This is a common measure giving values ranging from 0 to 1, where 1 is a perfect fit. The R^2 of the forebay level functions used in Model A:R are given in Figure 5.1. This shows that for most reservoirs, the selected fit is almost perfect to the data. Since a fit including more variables always produce a closer fit to the data (when the number of data points is sufficient), we can be sure that one of the selected fits from (4.17)-(4.20) always is better than the simplest linear (4.16) used in Model A and Model B.

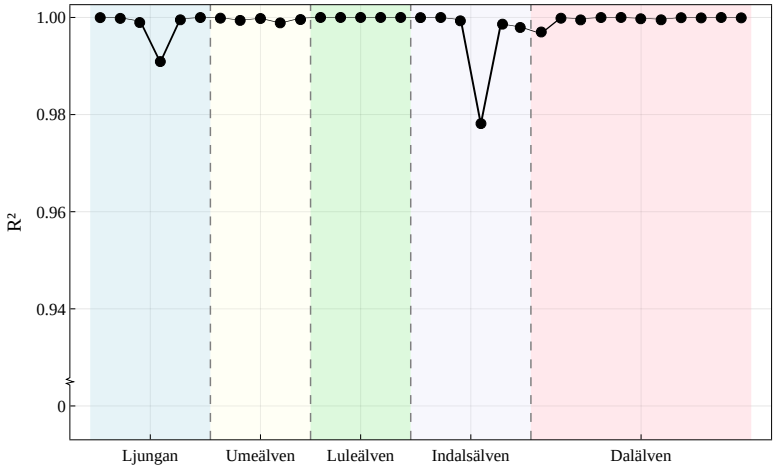

Figure 5.1: R^2 values for nonlinear fits across modeled reservoirs.

The difference in how the forebay levels are modeled between the old model, Model A, and the proposed models Model A:R and Model A:EQ can be measured by calculating the difference between the functions representing the forebay level:

Definition 5.1 (Forebay level difference) *Let $u(V)$ be a nonlinear forebay level function and $l(V)$ a linear. Then the forebay mean difference for a reservoir is defined as:*

$$\overline{\delta W^F} = \int_0^{v^{max}} \frac{u(V) - l(V)}{v^{max}} dV \cdot \frac{1}{w^{max} - w^{min}}$$

The forebay maximum difference for a reservoir n is defined as:

$$\delta W^F{}_{max} = \max_V \{u(V) - l(V)\} \cdot \frac{1}{w^{max} - w^{min}}$$

The first measure, forebay mean difference, is essentially the difference between the nonlinear and linear forebay level functions calculated for the volume $\bar{V}$ in the center of gravity of the integral and then normalized by dividing by the operating range. The second measure, forebay max difference, is the maximum possible difference normalized by the operating range of the reservoir. Figure 5.2b shows histograms of the differences for all the reservoirs in the five rivers.

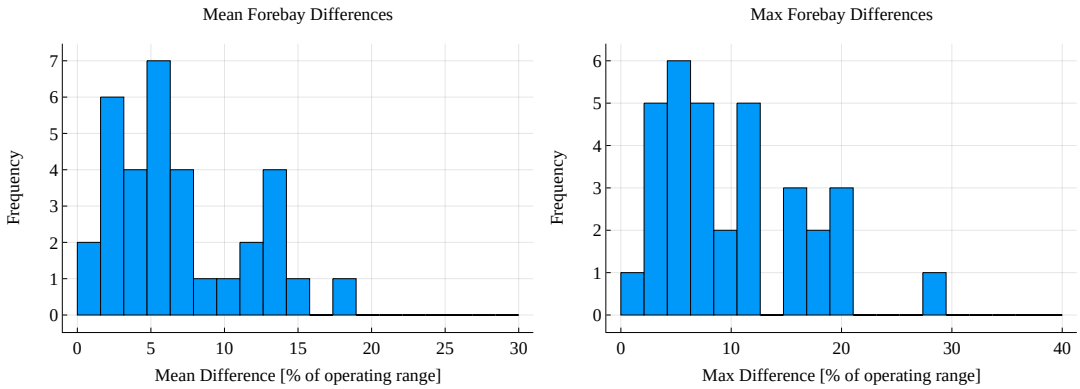

(a) Mean forebay level differences. **(b)** Max forebay level differences.

Figure 5.2: Histogram between the nonlinear fits and linear approximation for all 33 reservoirs with nonlinear reservoir curves.

The mean differences are scattered around 6 % of the operating range and the maximum differences around 7.5 %. As an example, a 6 % difference for a reservoir with 5 m operational range gives a difference of 30 cm. The largest absolute maximum difference found for a reservoir was greater than 6 m for a specific reservoir content. These results indicate that in order to capture more detailed forebay levels for correct scenario analysis, more intricate mathematical functions than a linear is required.

5.2 Model robustness validation

To verify the validity of Model A:R and Model B:R, where forebay levels are allowed to take less realistic values and then recalculating them post-optimization, they are compared with Model A:EQ and Model B:MILP respectively. The results in this section are answering research question number two: *In what ways can reservoir curves be implemented in a hydropower optimization model?* The methods to implement reservoir curves in hydropower optimization models are given in Section 4.3, the results presented here mean to show the robustness of the models Model A:R and Model B:R. To test the robustness of these model versions, they are evaluated for March during the dry year 2016 and wet year 2020, each with historical price data and extreme price profiles. The tests are limited to a one month horizon due to Model A:EQ and Model B:MILP being computationally difficult to solve for longer time periods.

As the models Model A:R and Model B:R represent the forebay levels with inequality constraints, the solutions from these models can allow reservoir forebay levels lower than the actual reservoir curve. An example of this occurring for Model A:R can be seen in Figure 5.3, a reservoir with a power plant where many of the forebay level values do not lie on the upper bound of the constraint before the solution is recalculated. Similar results are found for Model B:R before the solution is recalculated post-optimization. It should be noted that for the majority of the reservoirs, the forebay level values do follow the upper bound constraint, needing no post-optimization recalculation.

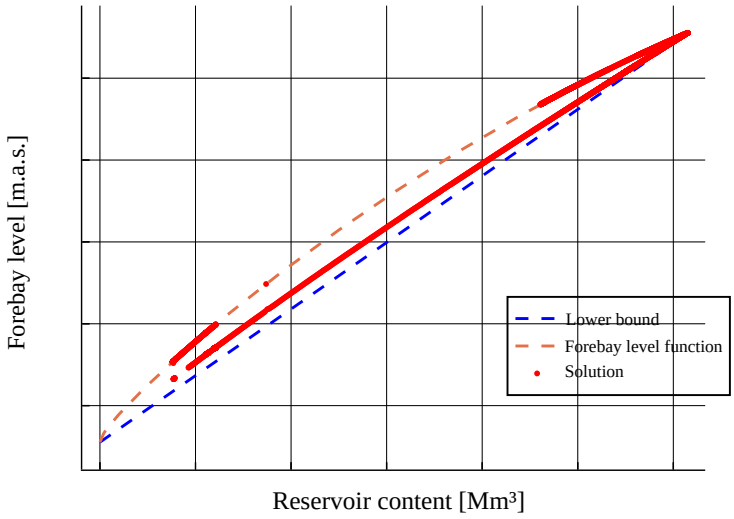

Figure 5.3: A demonstrative example of when a solution with Model A:R does not use the correct forebay levels in its solution before they are recalculated.

To validate whether Model A:R and Model B:R, where the solution is adjusted

post-optimization, is reliable in terms of full river scenario analysis. These models are compared with Model A:EQ and Model B:MILP respectively. The first metric to determine how close two solutions are is the relative optimality gap:

Definition 5.2 (Relative optimality gap (ROG)**)**

$$ROG = \frac{R^*_{GT} - R^*}{R^*} \cdot 100$$

where R^*_{GT} *is the revenue for the model used as ground truth to compare against and* R^* *the revenue for the compared model. The multiplication by 100 is to express the measure in percentage.*

The differences in relative optimality gap between Model A:R and Model A:EQ are generally small as seen in Figure 5.4, with the most relative optimality gaps being in the span of 0-0.1 %. The two standout cases are for Luleälven 2016 and 2020 with historical prices, indicating that there is a discrepancy between the models.

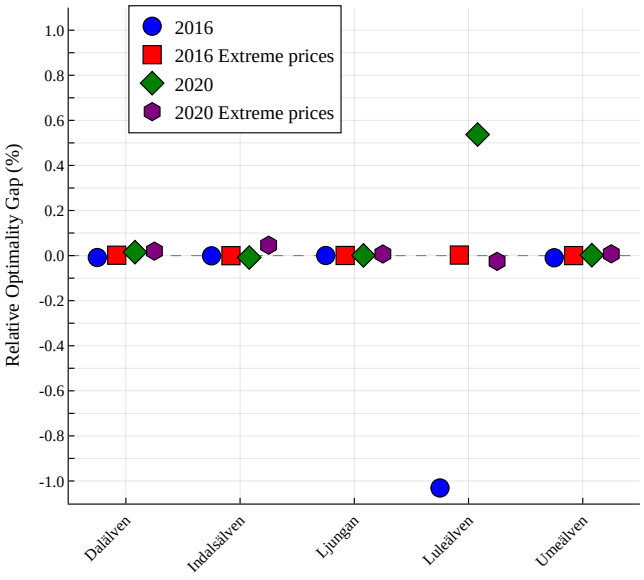

Figure 5.4: Relative Optimality gaps for Model A:R for March 2016 and 2020 with both regular and extreme price profiles.

To contextualize the relative optimality gap results from above, the two worst cases from Luleälven will be examined. Figure 5.5 shows the power duration curves (hourly power production ordered in descending order) for March in 2016 and 2020. In March 2016 the ROG is -1.1 % which means Model A:R found a better solution than Model A:EQ. The power production in these solutions were 1.648 TWh for Model A:R and 1.639 TWh for Model A:EQ. In 2020 the power production were 1.634 TWh and 1.633 TWh respectively, and 0.6 % ROG, meaning Model A:EQ found the better solution. These differences in optimal solutions are definitely not negligible.

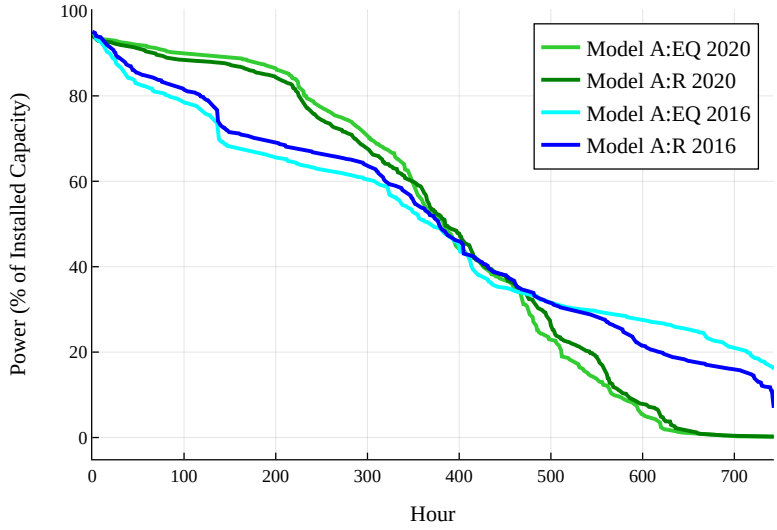

Figure 5.5: The cumulative power production for Model A:R compared with Model A:EQ for Luleälven in March 2016 and 2020.

We know from the theory in Section 3.4 that it is not possible to find global optimal solutions for nonlinear and nonconvex optimization problems in general, hence the solutions presented in Figure 5.4 are local optima. The results showing a negative ROG are likely due to Model A:EQ getting stuck at a poor local optimum, since solutions of Model A:R are feasible in Model A:EQ, we know that this model could have found an equally good solution. The results showing positive ROG are more what is expected since the post-optimization recalculation can give sub-optimal solutions when the forebay levels are recalculated. One such mechanism might be that when a forebay level is recalculated to a higher value, the upstream reservoir gets higher tailrace level (4.11), which in turn decreases the head (4.12).

Looking at the relative optimality gaps for Model B:R in Figure 5.6, Model B:MILP does not find a better feasible solution than the Model B:R solutions. The theory of MIP in Section 3.5 explains that the algorithms used in IP usually settle with a good enough solution. The best bound calculated by the solver is an upper bound for how high the revenue potentially can be for another solution if more branches in the solution tree were explored for Model B:MILP. The best bound comparisons show evidence that, while there may be a better solution to be found for some scenarios, the amount of potential difference between Model B:R and Model B:MILP is small. For all scenarios for Indalsälven and Umeälven (except 2020 with extreme prices) the best bound is equal to the Model B:R solutions, here we can say for certain that Model B:R behaves well.

The results of the linear models, showing that there are no realized and very small theoretical differences between the model versions Model B:MILP and Model B:R, indicates that the post-optimization recalculation is working. The benefit of LP is that a global optimum can always be found, as presented in Section 3.3. This makes

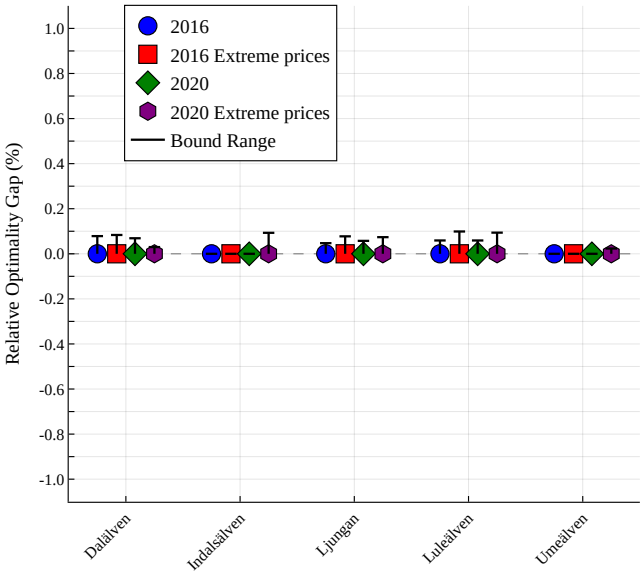

Figure 5.6: Relative optimality gaps for Model B:R for March 2016 and 2020 with both regular and extreme price profiles. Relative optimality gap is also shown for the best bound found in the Model B:MILP solution, this range shows where a potential better solution could have been found if the solver were run for longer.

it easier to confidently draw conclusions from these results, as they are not clouded with the insecurities of local optimums as the nonlinear models are. It is hard to say whether the differences between the nonlinear models are systematic or natural variances coming from local optimums. However, with the promising results of the linear models, we argue that the models Model A:R and Model B:R seem to be close enough to the exact models Model A:EQ and Model B:MILP to be useful.

5.3 Modeling of reservoir level environmental permits

Another result from modeling the forebay levels more accurately is that it allows using today's real environmental permits for the rivers evaluated, where the previous models could not handle all cases. This answers directly to research question three: *How does more detailed modeling of reservoir forebay levels affect the feasibility of modeling river hydropower environmental permits?*

The baseline model versions Model A and Model B are not feasible for some environmental permits and start and end times. The general explanation for this is that the models define constraints for the start and end reservoir contents to give meaningful solutions. This in combination with specific precipitation inflow data makes it impossible to reach certain reservoir levels when the forebay level follows a linear function as (4.10). This phenomenon is explained in Figure 2.4, where it is

clear that a forebay level following a linear function requires more water volume in the reservoir to reach a certain forebay level.

The number of infeasible scenarios is uncountable since many different start and end time combinations may produce an impossible scenario. One specific example is the permit that declares that the forebay level in the reservoir Leringsforsen in Ljungan river must be at least 200.5 m.a.s. in July and 201.5 m.a.s. in August. This was not feasible in the models Model A and Model B, but is now possible to model in Model A:R and Model B:R. A representation of the forebay levels and environmental constraints for Leringsforsen in Ljungan is presented in Figure 5.7.

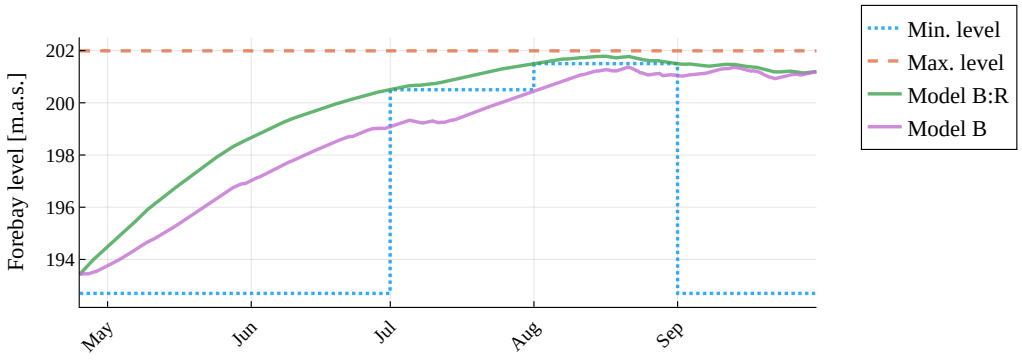

Figure 5.7: Forebay level in the reservoir Leringsforsen in Ljungan from an example scenario. Here the real environmental constraints are violated by the old but not the new models. This figure is constructed by running the Model B with a relaxed minimum level to enable a solution.

5.4 Full year model version comparisons

In this section, comparisons of the models Model A, Model A:R, Model B, and Model B:R are presented, answering the fourth research question: *How do more accurately modeled forebay levels affect modeled scenarios for large river networks?* The differences in physical representations between the models will be presented by comparing full year revenues and power duration curves for both aggregated river systems and individual power plants.

The new models Model A:R and Model B:R and the baseline models Model A and Model B are solved for the full years 2016 and 2020 using historical price profiles. The full revenues for each model, summarized over the five rivers (Table 4.2) are presented in Figure 5.8. Detailed revenue and power production results are included in Appendix A.

From the resulting total revenues of the full year solutions presented in Figure 5.8, we see that the revenues are very similar between the old and new model versions. This indicates that the impact of a more detailed modeling of forebay levels does not have a consequential impact on the potential aggregated revenue for whole rivers.

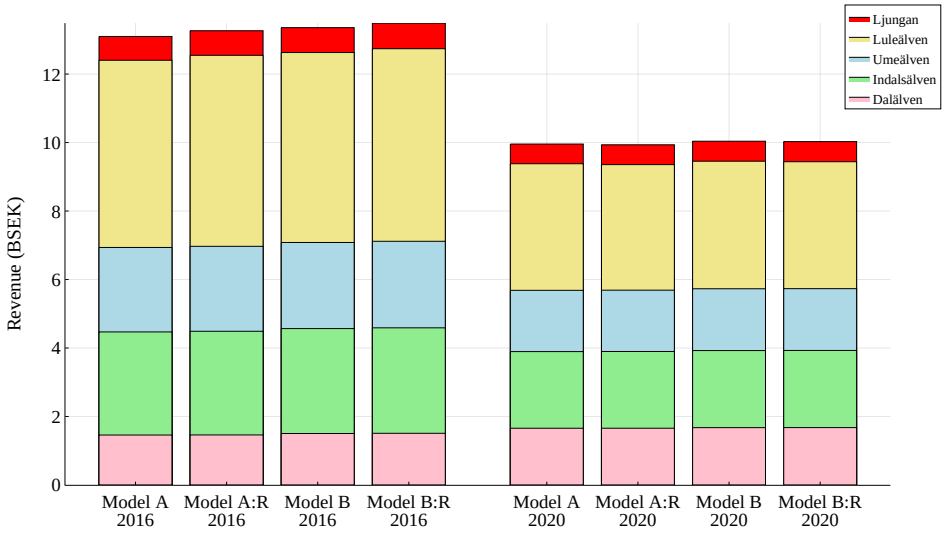

Figure 5.8: Full cumulated revenues for all five rivers summed over the years 2016 and 2020 respectively.

To further investigate whether a more accurate forebay representation has any effect on scenario analysis, the power duration curves aggregated across all rivers are presented for 2020 in Figure 5.9a (see Appendix B for a similar figure for 2020 and for linear models). The power duration curves do not differ notably, in 2016 Model A:R has slightly higher power production compared to Model A but in 2020 the reverse is true. However, the different forebay level modeling can have effects for the individual power plants. Figure 5.9b displays one case of a power plant where the power output differs, indicating that the effect on individual plants could be consequential (see Appendix C for more examples).

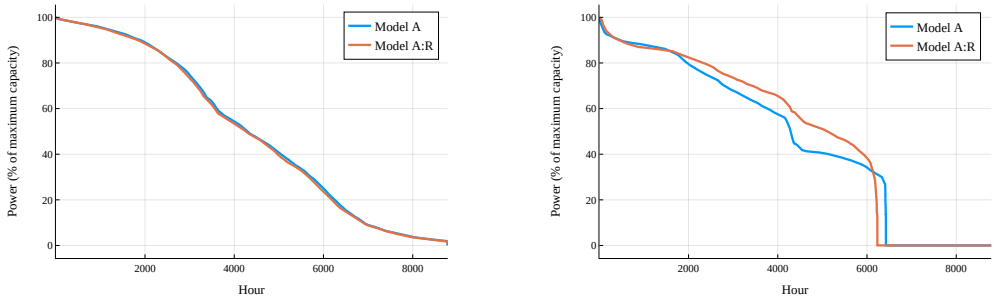

(a) Accumulated power duration curves for all five rivers.

(b) Power duration curves for the plant Parki in Umeälven.

Figure 5.9: Model A and Model A:R power duration curves for the year 2020.

The above results show that adding more detail to the forebay level modeling could influence the river network scenario analysis to some degree. Although aggregated results do not differ much between the old and new models, the differences

at plant level could be of interest. The power duration curves for individual plants presented in Figure 5.9b indicate that the detailed forebay level modeling has an impact on some plants. Of the 133 reservoirs in the dataset, only 33 have reservoir curves indicating a nonlinear relationship between the reservoir content and the forebay level. It is possible that the results presented would give larger differences for rivers with higher ratio of nonlinear reservoir curves and vice versa for rivers with a lower number of nonlinear reservoir curves.

Looking at the computational times (Figure 5.10) we can see that Model A:R does have slightly longer computational times in general compared to Model A but they are still tractable. The toughest problem to solve was Dalälven 2016 which took roughly 27 hours for Model A:R, bordering on what we consider to be a reasonable solve time. When comparing Model B:R against Model B we see that Model B:R is actually consistently faster than Model B. Since these solve times are in the range of 1-20 minutes, the actual speed increase in terms of seconds is not huge but still a nice result.

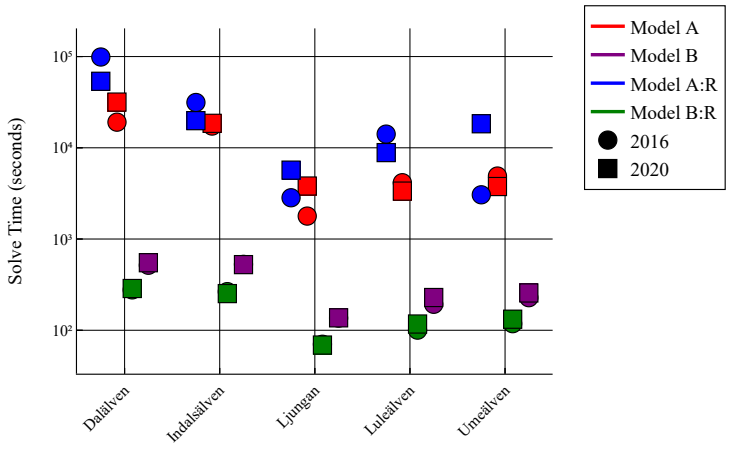

Figure 5.10: Computational times for Model A:R, and Model B:R, compared with Model A and Model B.

Nonlinear and nonconvex optimization is quite devious in the sense that it is not always clear what changes in a model make it more difficult or easy to solve. In some cases, more constraints can be helpful as local minima in the feasible region are excluded, but sometimes the opposite can be true where more relaxed constraints give the solver more freedom and are less prone to getting stuck at poor local optima. We suspect that one reason for the slower computational times in Model A:R is due to the inclusion of square root terms in the reservoir curve fits. Computing gradients of square root functions can be unstable for values close to zero, and optimization solvers are commonly better equipped to handle simple polynomials such as quadratic functions. This was not explored thoroughly in this work but could be a detail of further study.

6
Conclusion

The methods presented to mathematically represent reservoir forebay levels, which answer the first research question, work well for the investigated rivers. In this study, four different nonlinear fits were chosen, but naturally any type of fit can be incorporated when looking for a best fit to a reservoir curve. It was observed that incorporating fits with square root terms in the nonlinear model Model A:R might cause increased solve times. They were, however, very precise in terms of error to the reservoir curve data in many cases. This trade-off between finding the best possible functions to fit and keeping the models computationally feasible was not explored thoroughly, and future research might find more suitable functions. We can, although, conclude that more intricate functions than linear give more exact modeled forebay levels.

The second research question discusses how to incorporate these reservoir curve fits into the existing optimization models Model A and Model B. We propose four models Model A:R, Model A:EQ, Model B:R, and Model B:MILP which all succeed in formulating a more detailed forebay level function, but with different implications for computational effort. The model versions Model A:R and Model B:R are proposed as the best models in terms of trade-offs between accuracy and computational effort. If one is interested in coarser time resolution or shorter time periods, the models Model A:EQ and Model B:MILP could be more suitable.

The third research question aims to investigate whether models including more detailed forebay level modeling can incorporate environmental constraints successfully. The models Model A:R and Model B:R can incorporate environmental permits in the scenario analysis which the baseline models Model A and Model B failed to do in some cases. In order to take well informed decision when deciding new environmental permits, it is important to capture more exact forebay levels. Small differences in allowed forebay levels can potentially have large impacts on the capacity and flexibility of power plants, and the social and biological environment connected to the river systems.

As for the fourth and last research question, which seeks to analyze the impact on modeled results of including detailed reservoir modeling in full river network scenario analysis, our results point to two general conclusions. For a complete aggregated river network, including a more detailed forebay level does not show any notable differences in the scenarios evaluated, both in terms of total revenue and power production capacity. On the other hand, we have indications that the power production capacity of individual power plants in the river systems shows notable differences between the previous and new models. These indications show that, in order to draw correct conclusions from the scenario analysis at a power plant level,

the incorporation of detailed forebay levels in the model could be important.

In conclusion, we have successfully found methods to mathematically express reservoir curves and incorporate them into existing hydropower optimization models. Our proposed models Model A:R and Model B:R enable accurate modeling of environmental permits and we show that different operational patterns are found for individual plants in river systems. These different operational patterns, compared to when linear reservoir curves were assumed, can affect the power production capacity of individual plants. However, the aggregated effects on production patterns and revenue for a whole river are not consequential.

Bibliography

[1] International Hydropower Association. *2024 World Hydropower Outlook*. Accessed: 2025-04-17. June 2024. URL: https://www.hydropower.org/publications/2024-world-hydropower-outlook.

[2] Michael Child et al. "Flexible electricity generation, grid exchange and storage for the transition to a 100% renewable energy system in Europe". In: *Renewable Energy* 139 (2019), pp. 80–101. DOI: 10.1016/j.renene.2019.02.077. URL: https://www.sciencedirect.com/science/article/pii/S0960148119302319.

[3] IPCC Core Writing Team, H. Lee, and J. Romero, eds. *Climate Change 2023: Synthesis Report. Contribution of Working Groups I, II and III to the Sixth Assessment Report of the Intergovernmental Panel on Climate Change*. Geneva, Switzerland: IPCC, 2023, pp. 35–115. DOI: 10.59327/IPCC/AR6-9789291691647.

[4] Birgitta Malm Renöfält, Roland Jansson, and Christer Nilsson. "Effects of hydropower generation and opportunities for environmental flow management in Swedish riverine ecosystems". In: *Freshwater Biology* 55.1 (2010), pp. 49–67. DOI: https://doi.org/10.1111/j.1365-2427.2009.02241.x. URL: https://onlinelibrary.wiley.com/doi/abs/10.1111/j.1365-2427.2009.02241.x.

[5] European Parliament and Council. *Directive 2000/60/EC of 23 October 2000 establishing a framework for Community action in the field of water policy*. Official Journal L 327, 22.12.2000, pp. 1–73. Water Framework Directive. 2000. URL: https://eur-lex.europa.eu/legal-content/EN/TXT/?uri=CELEX:32000L0060.

[6] European Commission. *Infringement Decision December 2024*. Commission Decision INF/24/6006. Adopted 16 December 2024. 2024. URL: https://ec.europa.eu/commission/presscorner/detail/en/inf_24_6006?fbclid=IwZXh0bgNhZW0CMTAAAR4bZ4mB8wsfD0FcipBKMebmpnOnhLGF_ANNgizEW7j6q536I_rN-be-_UXiUA_aem_uJ-ZtXqP6Z-9Q7JC1eZSVQ.

[7] J. P. S. Catalão et al. "Nonlinear optimization method for short-term hydro scheduling considering head-dependency". In: *European Transactions on Electrical Power* 20.2 (2010), pp. 172–183. DOI: https://doi.org/10.1002/etep.301. URL: https://onlinelibrary.wiley.com/doi/abs/10.1002/etep.301.

[8] H. Ek Fälth et al. “Trade-offs between aggregated and turbine-level representations of hydropower in optimization models”. In: *Renewable and Sustainable Energy Reviews* 183 (2023). DOI: 10.1016/j.rser.2023.113406. URL: https://www.sciencedirect.com/science/article/pii/S1364032123002630.

[9] Chao Wang et al. “Long-term scheduling of large cascade hydropower stations in Jinsha River, China”. In: *Energy Conversion and Management* 90 (2015), pp. 476–487. ISSN: 0196-8904. DOI: https://doi.org/10.1016/j.enconman.2014.11.024. URL: https://www.sciencedirect.com/science/article/pii/S0196890414009819.

[10] Martin N. Hjelmeland, Arild Helseth, and Magnus Korpås. “Medium-Term Hydropower Scheduling with Variable Head under Inflow, Energy and Reserve Capacity Price Uncertainty”. In: *Energies* 12.1 (2019). ISSN: 1996-1073. DOI: 10.3390/en12010189. URL: https://www.mdpi.com/1996-1073/12/1/189.

[11] Mario T. L. Barros et al. “Optimization of Large-Scale Hydropower System Operations”. In: *Journal of Water Resources Planning and Management* 129.3 (2003), pp. 178–188. DOI: 10.1061/(ASCE)0733-9496(2003)129:3(178). URL: https://ascelibrary.org/doi/abs/10.1061/%28ASCE%290733-9496%282003%29129%3A3%28178%29.

[12] Tiantian Yang et al. “Improving the multi-objective evolutionary optimization algorithm for hydropower reservoir operations in the California Oroville–Thermalito complex”. In: *Environmental Modelling & Software* 69 (2015), pp. 262–279. DOI: https://doi.org/10.1016/j.envsoft.2014.11.016.

[13] Vineet Kumar Singh and S.K. Singal. “Operation of hydro power plants-a review”. In: *Renewable and Sustainable Energy Reviews* 69 (2017), pp. 610–619. ISSN: 1364-0321. DOI: https://doi.org/10.1016/j.rser.2016.11.169. URL: https://www.sciencedirect.com/science/article/pii/S1364032116309200.

[14] Q. Goor, R. Kelman, and A. Tilmant. “Optimal Multipurpose-Multireservoir Operation Model with Variable Productivity of Hydropower Plants”. In: *Journal of Water Resources Planning and Management* 137.3 (May 2011), pp. 258–267. ISSN: 0733-9496, 1943-5452. DOI: 10.1061/(ASCE)WR.1943-5452.0000117. URL: https://ascelibrary.org/doi/10.1061/%28ASCE%29WR.1943-5452.0000117 (visited on 04/07/2025).

[15] Ignacio Guisández, Juan I. Pérez-Díaz, and José R. Wilhelmi. “Assessment of the economic impact of environmental constraints on annual hydropower plant operation”. In: *Energy Policy* 61 (2013), pp. 1332–1343. ISSN: 0301-4215. DOI: https://doi.org/10.1016/j.enpol.2013.05.104. URL: https://www.sciencedirect.com/science/article/pii/S030142151300459X.

[16] Niclas Andréasson, Anton Evgrafov, and Michael Patriksson. *An Introduction to Continuous Optimization: Foundations and Fundamental Algorithms*. Lund: Studentlitteratur, 2016. ISBN: 9789144115290. URL: https://research.ebsco.com/c/lu54te/search/details/gdjuxlke3z?q=An%20introduction%20to%20continuous%20optimization.

[17] Stephen Boyd and Lieven Vandenberghe. *Convex Optimization*. Seventh printing with corrections 2009. First published 2004. Cambridge: Cambridge University Press, 2004. ISBN: 978-0-521-83378-3. URL: http://www.cambridge.org/9780521833783.

[18] John A Nelder and Roger Mead. "A simplex method for function minimization". In: *The computer journal* 7.4 (1965), pp. 308–313. DOI: https://doi.org/10.1093/comjnl/7.4.308.

[19] P. E. Gill et al. "On Projected Newton Barrier Methods for Linear Programming and an Equivalence to Karmarkar's Projective Method". In: *Mathematical Programming* 36 (1986), pp. 183–209. DOI: 10.1007/BF02592025. URL: https://doi.org/10.1007/BF02592025.

[20] Geoff Gordon and Ryan Tibshirani. "Karush-kuhn-tucker conditions". In: *Optimization* 10.725/36 (2012), p. 725.

[21] Jens Clausen. "Branch and bound algorithms-principles and examples". In: *Department of computer science, University of Copenhagen* (1999), pp. 1–30.

[22] Lawrence Livermore National Laboratory. *El Capitan: NNSA's First Exascale Machine*. Accessed: 2025-04-04. 2024. URL: https://asc.llnl.gov/exascale/el-capitan.

A

Model comparison results

Table A.1: Revenue, power production, and computational time for models Model B:R and Model B for dry year 2016 and wet year 2020.

River-Model	Revenue (MSEK)	Prod. (TWh)	Time (s)
Dry year 2016			
Ljungan-Model B:R	746.79	2.24	70.22
Ljungan-Model B	726.61	2.22	135.87
Umeälven-Model B:R	2527.37	7.73	118.09
Umeälven-Model B	2514.84	7.71	227.59
Luleälven-Model B:R	5624.08	16.32	100.31
Luleälven-Model B	5546.45	16.08	192.62
Indalsälven-Model B:R	3080.04	9.42	265.15
Indalsälven-Model B	3063.55	9.39	527.70
Dalälven-Model B:R	1509.29	4.59	277.09
Dalälven-Model B	1503.84	4.59	515.85
Wet year 2020			
Ljungan-Model B:R	586.94	2.60	68.88
Ljungan-Model B	583.60	2.60	136.81
Umeälven-Model B:R	1804.12	9.39	132.23
Umeälven-Model B	1804.64	9.43	256.37
Luleälven-Model B:R	3707.30	15.83	117.13
Luleälven-Model B	3725.13	16.07	228.58
Indalsälven-Model B:R	2253.07	11.15	252.28
Indalsälven-Model B	2251.31	11.20	524.22
Dalälven-Model B:R	1675.98	5.52	286.87
Dalälven-Model B	1674.30	5.50	549.71

Table A.2: Revenue, power production, and computational time for models Model A:R Model A for dry year 2016 and wet year 2020.

River-Model	Revenue (MSEK)	Prod. (TWh)	Time (s)
Dry year 2016			
Ljungan-Model A:R	717.37	2.11	2834.02
Ljungan-Model A	694.46	2.08	1784.71
Umeälven-Model A:R	2480.94	7.52	3054.10
Umeälven-Model A	2466.35	7.50	4901.22
Luleälven-Model A:R	5578.01	16.05	14126.77
Luleälven-Model A	5467.08	15.71	4143.02
Indalsälven-Model A:R	3027.62	9.24	31376.63
Indalsälven-Model A	3011.01	9.21	17310.17
Dalälven-Model A:R	1461.39	4.40	98854.85
Dalälven-Model A	1458.98	4.41	19087.73
Wet year 2020			
Ljungan-Model A:R	578.76	2.50	5691.28
Ljungan-Model A	574.31	2.50	3810.96
Umeälven-Model A:R	1790.43	9.25	18332.43
Umeälven-Model A	1789.31	9.29	3761.46
Luleälven-Model A:R	3666.58	15.41	8856.61
Luleälven-Model A	3697.13	15.75	3350.48
Indalsälven-Model A:R	2240.92	11.02	19830.14
Indalsälven-Model A	2238.04	11.08	18549.03
Dalälven-Model A:R	1657.78	5.37	53596.05
Dalälven-Model A	1657.37	5.38	31694.28

B

Aggregated power duration curves

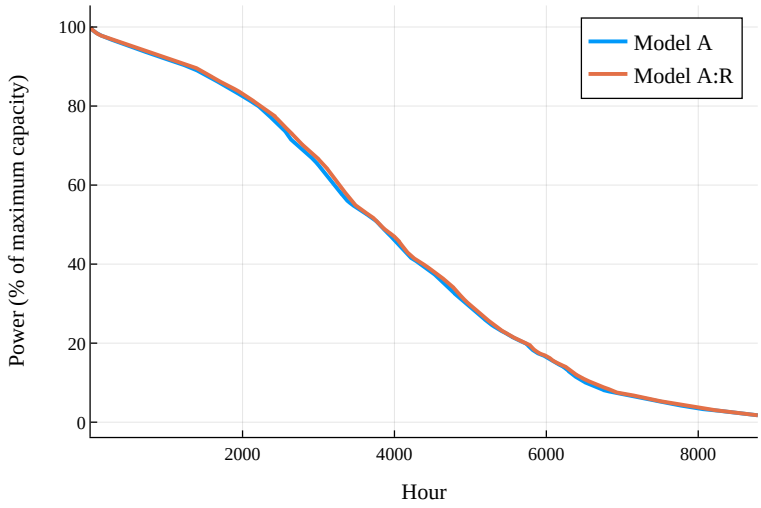

Figure B.1: Model A:R and Model A Power duration curves accumulated across all rivers for year 2016

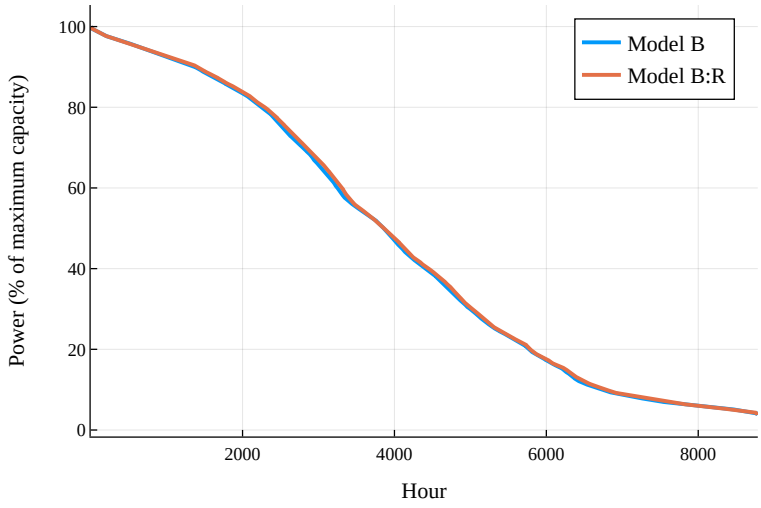

Figure B.2: Model B:R and Model B Power duration curves accumulated across all rivers for year 2016

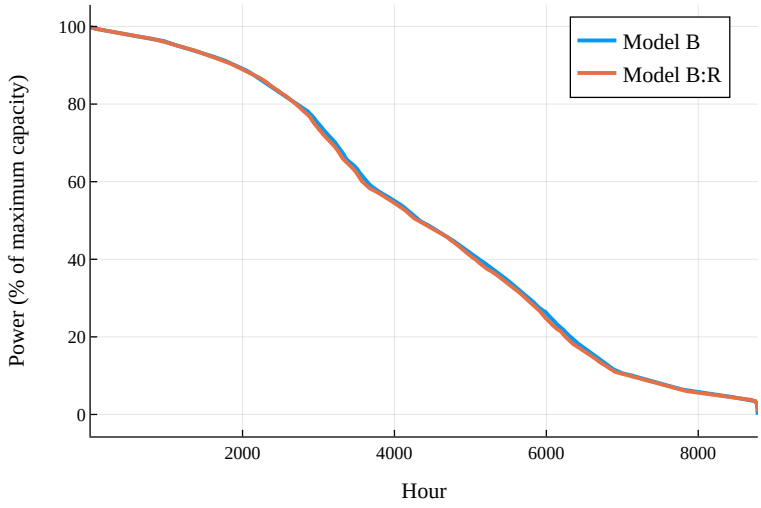

Figure B.3: Model B:R and Model B Power duration curves accumulated across all rivers for year 2020

C

Individual plant power duration curves

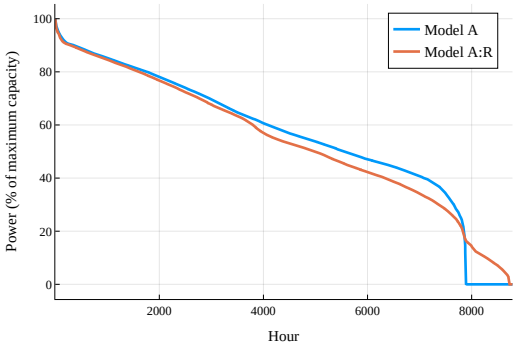

(a) Avestaforsen in the river Dalälven.

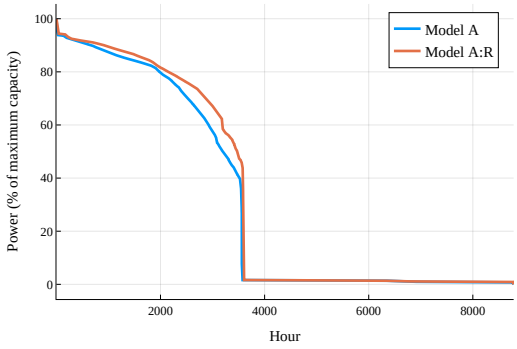

(b) Flåsjön in the river Ljungan.

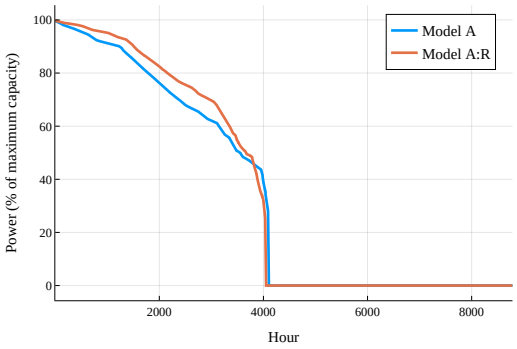

(c) Leringsforsen in the river Ljungan.

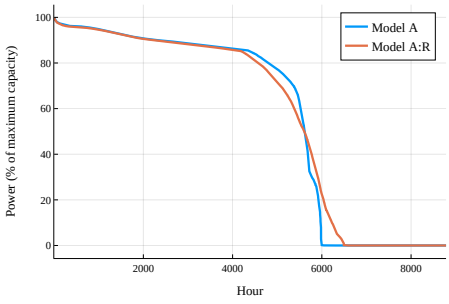

(d) Pengfors in the river Umeälven.

Figure C.1: Some examples of individual power plant power duration curves which differ between the new Model A:R and baseline Model A for year 2020.

DEPARTMENT OF SPACE, EARTH AND ENVIRONMENT
CHALMERS UNIVERSITY OF TECHNOLOGY
Gothenburg, Sweden
www.chalmers.se

CHALMERS
UNIVERSITY OF TECHNOLOGY